2016

Energy Constrained Shortest-Time Maneuvers for Reaction Wheel Satellites

Marsh, Harleigh C.; Karpenko, Mark; Gong, Qi

AIAA

Marsh, Harleigh, Mark Karpenko, and Qi Gong. "Energy constrained shortest-time maneuvers for reaction wheel satellites." AIAA/AAS astrodynamics specialist conference. 2016.

http://hdl.handle.net/10945/65782

AIAA SPACE Forum
13 - 16 September 2016, Long Beach, California
AIAA/AAS Astrodynamics Specialist Conference

10.2514/6.2016-5579

Energy Constrained Shortest-Time Maneuvers for Reaction Wheel Satellites

Harleigh C. Marsh*
University of California Santa Cruz, Santa Cruz, California 95064

Mark Karpenko†
Naval Postgraduate School, Monterey, California 93943

and

Qi Gong‡
University of California Santa Cruz, Santa Cruz, California 95064

In this paper we develop energy-metrics that are in-line with true energy costs incurred when performing a slew using reaction wheels. These energy-metrics are incorporated in constrained nonlinear optimal control formulations, which enable detailed analysis on the relationship between transfer-time and energy to be performed. Through numerical simulations, a nonlinear relationship between transfer time and minimal energy is used to help explain the tradeoff between transfer time and energy consumption. This analysis can provide important information for design and operations. In examining the relationship between transfer-time and minimal energy, we also analyze the difference between off-eigenaxis and conventional eigenaxis maneuvering. It is demonstrated that, by deviating from rotations about an eigenaxis the transfer-time may be significantly decreased but without incurring more energy than an eigenaxis maneuver. Analogously, energy may be reduced for an eigenaxis maneuver.

I. Introduction

Attitude control of spacecraft that utilize reaction wheels (RWs) has been an active research area for many years. This paper focuses on minimizing the energy consumption of a spacecraft over the course of a slewing-maneuver. The manner in which this problem is approached, is through an optimal control framework to allow the utilization of the recent advances made in pseudospectral (PS) methods for optimal control.[1–6] Another reason for choosing an optimal control framework in which to pose the optimization problem is that solutions derived from PS optimal control methods have been shown to be successfully implemented in flight, as seen from the landmark achievements of the Zero Propellant Maneuver of the International Space Station,[7–9] and the first flight-implementation of a shortest-time slew maneuver.[10–12]

Existing research on minimum energy attitude maneuvers for RW spacecraft has been addressed from a multitude of approaches concerning the way energy usage is modeled, and whether the energy is minimized instantaneously (local) or over an entire trajectory (global). In Refs.[13, 14] the local approach was taken, and feedback solutions were developed to minimize the total mechanical energy consumed by spacecraft consisting of a redundant (four or more) set of RWs. In Ref.[13] and Ref.[14], the emphasis is on how to effectively map a required control torque determined by a given attitude control law to a set of reaction wheel motor torques. In Ref.[13] total power was modeled as the L_1 norm of mechanical power of the reaction wheels. In Ref.[14] total power was modeled wherein mechanical energy may be extracted when braking a wheel.

*H. C. Marsh is a graduate student at the Univ. of California, Santa Cruz, CA, 95064. Email: hcmarsh@soe.ucsc.edu
†M. Karpenko is a Research Associate Professor of Mechanical and Aerospace Engineering at the Naval Postgraduate School, Monterey, CA 93943. Email: mkarpenk@nps.edu
‡Q. Gong is an Associate Professor of Applied Mathematics and Statistics at the Univ. of California, Santa Cruz, CA, 95064. Email: qigong@soe.ucsc.edu

The global approach, which requires knowledge of the initial and final states as well on an entire trajectory in between, have been posed in an optimal control framework.[15–17] Ref.[15] applied variational methods for a single reaction wheel for a spacecraft performing a small angle slew. The small angle slew warranted linear plant-dynamics, where the cost function minimizes only the copper-loss (i.e. current-squared times resistance) of the reaction wheel. Ref.[16] considered the single reaction wheel model and applied the variational form of optimal control, but for a large slew so the plant-dynamics are nonlinear. In this case, a quadratic performance index was taken as the mechanical-power of the reaction wheel squared. A direct extension of Ref.[16], Ref.[17] presented a three wheel model and revisited the single wheel case, under a time varying RW torque constraint. Pontryagin's Minimum Principle was applied to generate a two-point boundary value problem to which was then solved numerically using a relaxation technique.[18]

The mechanical-power model has achieved some success in relation to energy minimization for attitude control. However when the total energy consumed by the RWs is modeled as the L_1 norm of the mechanical power, electrical power consumption is neglected but could be significant. For example, over the course of a maneuver, the motor alternates between acting as a load and acting as a source. In this paper, the total amount of electric-energy consumed to complete a slewing-maneuver is derived by identifying, at each instant of time, whether a motor is acting as a consumer or a generator. Such a metric is more in-line with the actual cost in energy to perform a slew, and is a key component of the optimal control problem formulation presented in this paper. Using this metric, new results for minimum energy slews are presented. A fixed-endpoint time-bounded optimal control problem is formulated for a rest-to-rest maneuver with the goal of minimizing electrical energy used by the reaction wheels. The formulation directly considers the nonlinear dynamics of the rotating spacecraft, along with state and control constraints pertinent to an operational environment; for example, specifying the starting and ending reaction wheel speeds, and enforcing bounds upon the achievable-torque and maximum speed of each of the reaction wheels, as well as imposing saturation limits upon the rate-gyros. The minimum energy optimal control problem is solved by the application of pseudospectral optimal control theory implemented in the software-package DIDO,[2] with verification of the necessary conditions of optimality arising from Pontryagin's Minimum Principal.

The remainder of this paper is organized as follows: First, the rotational dynamics for a spacecraft utilizing RWs is reviewed, and the metrics associated to electrical energy are derived. Next, an optimal control problem is formulated to minimize the electrical energy required to perform a rest-to-rest maneuver under various constraints in line with an operational setting. The necessary conditions to optimality attained from an application of Pontryagin's Minimum Principal are presented. Lastly, two sets of simulations are presented to demonstrate minimal electrical-energy attitude maneuvers, as well as to identify the relationship between transfer time and energy required to perform a maneuver under both eigenaxis and off-eigenaxis cases. The first simulation studies a single large angle slew, and the second simulation considers a five-point multislew which allows the energy and time relationship to be evaluated over a large operational envelope. From each set of simulations, a trade space of energy and transfer time between eigenaxis and off-eigenaxis maneuvering-types is identified and explored.

II. Dynamic Modeling

In this section both the rotational dynamics of the spacecraft and the metrics for electrical energy are derived. Each section is an integral part in the optimal control problem formulation presented in Section III.

A. Spacecraft Model

The rotational dynamics of a spacecraft with N_{rw} reaction wheels are derived through an application of Euler's equation of motion. The total angular momentum $H \in \mathbb{R}^3$ of the spacecraft system with respect to the body frame is decomposed as

$$H = H_{sc} + H_{rw}, \tag{1}$$

where $H_{sc} \in \mathbb{R}^3$ is the total angular momentum of the spacecraft, $H_{rw} \in \mathbb{R}^3$ is the total angular momentum of the reaction wheels. Each H_{sc} and H_{rw} are with respect to the body frame. Expanding the components in Eq. (1), the total angular momentum of the spacecraft is given as

$$H_{sc} = J_{sc}\omega, \tag{2}$$

where $J_{sc} \in \mathbb{R}^{3\times3}$ is the spacecraft inertia tensor and $\omega \in \mathbb{R}^3$ is the angular velocity of the spacecraft expressed in the body frame. Next, the total angular momentum of the reaction wheels given by the following equation:

$$H_{rw} = Ah_{rw}, \tag{3}$$

where $A = [a_1|\cdots|a_{N_{rw}}] \in \mathbb{R}^{3\times N_{rw}}$ is a projection matrix from the reaction wheel actuator frame to the spacecraft body frame, and $h_{rw} \in \mathbb{R}^{N_{rw}}$ is the angular momentum of each reaction wheel about its spin axis. Defining $J_{rw} \in \mathbb{R}^{N_{rw}\times N_{rw}}$ as a diagonal matrix whose i-th entry along the main diagonal is the inertia of the i-th reaction wheel, and defining the angular rate of the reaction wheel relative to its spin axis as $\Omega_{rw} \in \mathbb{R}^{N_{rw}}$ gives

$$h_{rw} = J_{rw}\big(\Omega_{rw} + A^{\mathsf{T}}\omega\big), \tag{4}$$

where the terms $A^{\mathsf{T}}\omega$ account for the angular momentum increment resulting from the motion of the spacecraft. Since $\Omega_{rw,i} \gg a_i^{\mathsf{T}}\omega$ for each $i = 1,\ldots,N_{rw}$, Eq. (4) is approximated as

$$h_{rw} = J_{rw}\Omega_{rw}. \tag{5}$$

The time rate of change with respect to the inertial frame for Eq. (2), and Eq. (3) under the approximation given in Eq. (5), is found through an application of the transport theorem,[19] assuming that J_{sc}, J_{rw}, and A are time-invariant with respect to the body frame:

$$\dot{H}_{sc} = J_{sc}\dot{\omega} + \omega \times J_{sc}\omega, \tag{6}$$

$$\dot{H}_{rw} = A\tau_{rw} + \omega \times AJ_{rw}\Omega_{rw}, \tag{7}$$

where $\tau_{rw} \in \mathbb{R}^{N_{rw}}$ is the torque generated by each reaction wheel about its spin axis. Assuming the absence of external disturbance torques, angular momentum is conserved and the time rate of change to the system's total angular momentum with respect to the inertial frame is zero. Applying the transport theorem upon Eq. (1) and substituting Eqs. (6),(7) gives

$$J_{sc}\dot{\omega} = -A\tau_{rw} - \omega \times (J_{sc}\omega + AJ_{rw}\Omega_{rw}). \tag{8}$$

Therefore, from Eq. (8) along with the derivative of Eq. (5), given as

$$\tau_{rw} = J_{rw}\dot{\Omega}_{rw}, \tag{9}$$

the rotational dynamics of the spacecraft with N_{rw} wheels are presented in matrix-form:

$$\begin{bmatrix} \dot{\omega} \\ \dot{\Omega}_{rw} \end{bmatrix} = \begin{bmatrix} J_{sc}^{-1}(-A\tau_{rw} - \omega \times (J_{sc}\omega + AJ_{rw}\Omega_{rw})) \\ J_{rw}^{-1}\tau_{rw} \end{bmatrix}.$$

To complete the spacecraft model, the attitude of the spacecraft is modeled using quaternions parameterized as

$$q = \left[e_1 \sin\left(\frac{\Phi}{2}\right),\ e_2 \sin\left(\frac{\Phi}{2}\right),\ e_3 \sin\left(\frac{\Phi}{2}\right),\ \cos\left(\frac{\Phi}{2}\right)\right]^{\mathsf{T}} \in \mathbb{R}^4,$$

where $e = [e_1, e_2, e_3]^{\mathsf{T}}$ is the eigenaxis and Φ is the rotation angle about the eigenaxis. The quaternion kinematic differential equations are described by the following system [20]:

$$\dot{q} = \frac{1}{2}\mathcal{Q}(\omega)q, \tag{10}$$

where $\mathcal{Q}(\omega)$ is a skew-symmetric matrix given as

$$\mathcal{Q}(\omega) \triangleq \begin{bmatrix} 0 & \omega_3 & -\omega_2 & \omega_1 \\ -\omega_3 & 0 & \omega_1 & \omega_2 \\ \omega_2 & -\omega_1 & 0 & \omega_3 \\ -\omega_1 & -\omega_2 & -\omega_3 & 0 \end{bmatrix}.$$

Quaternions are a redundant attitude parameterization, and so increase the dimension of the system's state by one when compared to non-redundant three-parameter attitude representations. Quaternions are, however, free of singularities or discontinuities inherit to three-parameter representations,[21] and so are well-suited for arbitrary large-angle slews. Since no trigonometric relations appear in the kinematic differential equations described in Eq. (10), rather only products, quaternions are befitting for on-board real-time computation,[20] and have been implemented in spacecrafts such as Galileo, HEAO (High Energy Astronomy Observatory), the space shuttle,[22] as well as in TRACE.[10]

B. Electrical Energy Model and Energy Metrics

The electric motor of a reaction wheel is modeled as a direct-current (DC) motor in steady state, where the load-torque is taken as the sum of commanded-torque, τ_{cmd}, and a friction term, and the angular velocity of the motor shaft is taken as the speed of the reaction wheel, Ω:

$$V = IR + K_V\Omega,$$
$$K_T I = \tau_{cmd} + \beta\Omega.$$

In the above equations, V is armature voltage, I is the armature current, R is the armature resistance, K_V is the back electromotive force (EMF) constant, K_T is the torque constant, β is the viscous friction coefficient. For SI units we note that $K_T = K_V$. When determining the electrical power at any instant in time, three terms appear: an armature copper-loss term which represents power lost as heat in the windings, a mechanical power term, and a term representing the amount of power loss due to friction:

$$\begin{aligned}\mathcal{P}_{elec}(t) &= V(t)I(t) = I^2(t)R + K_V\Omega(t)I(t),\\ &= \underbrace{\frac{R}{K_T^2}(\tau_{cmd}(t) + \beta\Omega(t))^2}_{\text{Copper Loss}} + \overbrace{\tau_{cmd}(t)\Omega(t)}^{\text{Mechanical Power}} + \underbrace{\beta\Omega^2(t)}_{\text{Friction Loss}}.\end{aligned}$$

Throughout the course of a maneuver, each motor may alternate between being a load ($\mathcal{P}_{elec,i}(t) > 0$) or being a source ($\mathcal{P}_{elec,i}(t) < 0$). In a regenerative setting, the battery can be charged when the motor is acting as a source.[23,24] In practice, regenerative methods are not implemented, so when a motor acts as a source, it is shunted to ground. From the above, a metric which measures the total electric power exerted at any time instance for N_{rw} reaction wheels, is given as:

$$\mathcal{P}_{elec}(t) = \sum_{i=1}^{N_{rw}} \{V_i(t)I_i(t)\}^+, \tag{11}$$

where $\{\cdot\}^+$ is defined as

$$\{f(t)\}^+ = \begin{cases} f(t) & \text{if } f(t) > 0 \\ 0 & \text{if } f(t) \leq 0 \end{cases}.$$

Integrating Eq. (11) over the transfer time $[0, T]$ represents the total electrical-energy required to perform the slew:

$$\mathcal{E}_{elec}^+ = \int_0^T \mathcal{P}_{elec}(t)\, dt. \tag{12}$$

Although $\mathcal{E}_{elec}^+$ represents the electrical energy consumed when performing a maneuver, taking $\mathcal{E}_{elec}^+$ as the cost functional in optimal control problem poses a numerical challenge, in that $\mathcal{P}_{elec}$ is a non-smooth function. Instead of mollifying $\mathcal{E}_{elec}^+$, a new metric is instead considered which measures the electrical power under the assumption of a 100 percent regenerative scheme. This regenerative-scheme metric is simply given as the summation of the individual electrical powers:

$$\mathcal{P}_{elec}^{rgn}(t) = \sum_{i=1}^{N_{rw}} V_i(t)I_i(t). \tag{13}$$

Under Eq. (9), the following relation is arrived upon by an application of integration by parts:

$$\int_0^T \sum_{i=1}^{N_{rw}} \tau_{rw,i}(t)\Omega_{rw,i}(t)\, dt = \sum_{i=1}^{N_{rw}} \frac{J_{rw,i}}{2}\left(\Omega_{rw,i}^2(T) - \Omega_{rw,i}^2(0)\right), \tag{14}$$

where $J_{rw,i}$ is the inertia of the i-th reaction wheel. When the starting and ending wheel speeds are fixed for each maneuver, Eq. (14) is a fixed constant. Integrating Eq. (13) in the situation where a slew begins and

ends with the same wheel bias (i.e. all reaction wheels start and end at the same speed) yields the following simplified energy metric:

$$\mathcal{E}_{elec}^{rgn} = \int_0^T \mathcal{P}_{elec}^{rgn}(t)\,dt = \int_0^T \sum_{i=1}^{N_{rw}} \left(\frac{R}{K_T^2}(\tau_{rw,i}(t) + \beta\Omega_{rw,i}(t))^2 + \beta\Omega_{rw,i}^2(t) \right) dt. \tag{15}$$

Equation (15) is the energy required to perform a slew under a 100 percent electric-regenerative scheme under the condition of a matching starting and ending bias for each wheel. But, $\mathcal{E}_{elec}^{rgn}$ serves as a secondary metric as well, measuring the cumulative amount of energy lost as heat occurring in the windings and energy lost as heat due to overcoming friction. This is seen from Eq. (15), as $\mathcal{E}_{elec}^{rgn}$ is the summation of the copper-loss and friction-loss term for each reaction wheel motor.

For the analysis given in this paper, the following two metrics will thus be useful:

$$\mathcal{C}_{loss} = \int_0^T \sum_{i=1}^{N_{rw}} I_i^2(t) R\,dt, \tag{16}$$

$$\mathcal{F}_{loss} = \int_0^T \sum_{i=1}^{N_{rw}} \Omega_{rw,i}^2(t)\beta\,dt. \tag{17}$$

Equations (16) and (17) represent the cumulative electric-energy lost in the motor windings, $\mathcal{C}_{loss}$, and cumulative electric-energy lost due to friction incurred by the reaction wheel motors, $\mathcal{F}_{loss}$, over the course of a slew.

III. Minimum Energy Maneuvers

A. Optimal Control Problem Formulations

In this section, a time-bounded optimal control problem formulation is developed for minimizing the electrical energy required for a spacecraft with N_{rw} reaction wheels to perform a rest-to-rest reorientation from an initial orientation $q^0 \triangleq \left[e_0 \sin\left(\frac{\Phi_0}{2}\right), \quad \cos\left(\frac{\Phi_0}{2}\right)\right]^\mathsf{T} \in \mathbb{R}^4$ to a final orientation $q^f \triangleq \left[e_f \sin\left(\frac{\Phi_f}{2}\right), \quad \cos\left(\frac{\Phi_f}{2}\right)\right]^\mathsf{T} \in \mathbb{R}^4$. Along with the relevant nonlinear spacecraft dynamics derived in Section II, the formulation incorporates constraints upon both the state and the control that are in-line with an operational scenario: i) The starting and ending reaction wheel speeds are set to the same speed-bias Ω_{bias}. ii) Maximum limits are imposed upon the spacecraft body to avoid saturation of the rate-gyros. If saturation of the rate-gyros occur, the result is the loss of control of the spacecraft. The real positive parameter ω_{max} represents the speed-bound for each spacecraft body axis. iii) Hardware constraints are placed upon the reaction wheels concerning the maximum amount of speed Ω_{max}, and maximum torque τ_{max} attainable for each reaction wheel. The optimal control problem formulation presented as follows, and is hereafter referred to as the Minimum-Energy (ME) formulation:

$$\text{(ME)} \begin{cases} \text{State:} & x = [q, \omega, \Omega_{rw}]^\mathsf{T} \in \mathbb{R}^{7+N_{rw}}, \quad \text{Control:} \quad \tau_{rw} \in \mathbb{R}^{N_{rw}}, \quad t_f: \text{ free} \\ \text{Minimize:} & J\left[x(\cdot), \tau_{rw}(\cdot), t_f\right] = \displaystyle\int_0^{t_f} \sum_{i=1}^{N_{rw}} \left(\frac{R}{K_T^2}(\tau_{rw,i}(t) + \beta\Omega_{rw,i}(t))^2 + \beta\Omega_{rw,i}^2(t) \right) dt \\ \text{Subject To:} & \\ & \begin{bmatrix} \dot{q} \\ \dot{\omega} \\ \dot{\Omega}_{rw} \end{bmatrix} = \begin{bmatrix} \frac{1}{2}\mathcal{Q}(\omega)q \\ J_{sc}^{-1}(-A\tau_{rw} - \omega \times (J_{sc}\omega + AJ_{rw}\Omega_{rw})) \\ J_{rw}^{-1}\tau_{rw} \end{bmatrix} \\ & 0 \le t_f \le T \\ & x(0) = \begin{bmatrix} q^0 & 0 & \Omega_{bias} \end{bmatrix}^\mathsf{T} \in \mathbb{R}^{7+N_{rw}} \\ & x(t_f) = \begin{bmatrix} q^f & 0 & \Omega_{bias} \end{bmatrix}^\mathsf{T} \in \mathbb{R}^{7+N_{rw}} \\ & |\omega_i| \le \omega_{max}, \ \forall\, i = 1, 2, 3 \\ & |\Omega_{rw,i}| \le \Omega_{max}, \ \forall\, i = 1, \ldots, N_{rw} \\ & |\tau_{rw,i}| \le \tau_{max}, \ \forall\, i = 1, \ldots, N_{rw} \end{cases} \tag{18}$$

The state of the system consists of the attitude of the spacecraft, angular velocity of the spacecraft body, and angular velocities of the reaction wheels (about their individual spin-axis). The control is taken as the torque generated by the reaction wheels. The upper bound on the time to complete the slew is given by T. It is a fixed constant satisfying $t_{STM} \leq T$, where t_{STM} represents the transfer-time of the shortest-time maneuver based on the slew with the same parameters and boundary conditions. A shortest-time maneuver is solved by freeing the final time t_f and setting the objective function to transfer time; for an in-depth presentation on shortest-time maneuvers, see Refs.[2, 10, 11, 25]. Choosing $\mathcal{P}_{elec}^{rgn}$ as the running cost results in a smooth objective functional, given as $\mathcal{E}_{elec}^{rgn}$ in Eq. (15). By minimizing $\mathcal{E}_{elec}^{rgn}$, the problem formulation reduces the energy consumption of spacecraft systems which can restore energy into the battery, but it will be shown later that this cost functional also significantly reduces the electrical energy for non-regenerative systems. Thus, our results are applicable to practical systems. Another physical interpretation of the performance index $\mathcal{E}_{elec}^{rgn}$ given as follows: Because $\mathcal{E}_{elec}^{rgn}$ measures the cumulative copper and friction losses incurred in the reaction wheel motors over the course of performing a slew, and since electrical losses are dissipated as heat, the performance index given in Eq. (18) searches for maneuvers which generate the least amount of dissipative loss.

In the numerical simulations to follow, the maneuvers attained by solving the ME formulation are compared against three other maneuvers, which are attained from three different optimal control problem formulations. These three maneuver-types are Shortest-Time off-eigenaxis and Eigenaxis maneuvers (denoted STMs and ST-EAMs), and Minimal Energy Eigenaxis maneuvers (denoted ME-EAMs). For the sake of brevity, these three problem formulations are defined by identifying the changes to the ME formulation. The Shortest-Time Maneuver (STM) problem formulation has two alterations to the ME formulation: i) The transfer time t_f is now free, thus removing the constraint $0 \leq t_f \leq T$. And, ii) The cost functional is now set to just the transfer time

$$J_{STM}\left[x(\cdot), \tau_{rw}(\cdot), t_f\right] = t_f.$$

To achieve an eigenaxis maneuver under a slew-rate constraint, the ME formulation requires two alterations: i) To constrain the movement of the spacecraft to be an EAM, the angular velocity of the spacecraft body must be collinear to the eigenaxis,[26] e, at each time instance throughout the maneuver. This corresponds to the following path-constraint added to the ME formulation:

$$\omega(t) \times e = 0 \in \mathbb{R}^3, \ \forall t.$$

Next, ii) To enforce the slew constraint, which limits the rate at which the spacecraft may be rotated about the eigenaxis, the individual angular velocity constraints $|\omega_i| \leq \omega_{max}, \ \forall\, i = 1, 2, 3$, in ME is replaced by the following two-norm path-constraint:

$$\|w\|_2 \leq \omega_{max}.$$

Therefore, a Minimal Energy Shortest-Time Maneuver (ME-STM) is arrived-upon by solving the ME formulation whose transfer time is set that of the STM. In similar manner, a ST-EAM is a Shortest-Time eigenaxis maneuver, and is determined by solving the shortest-time formulation where the motion of the spacecraft is limited to be an EAM. Similarly a Minimal Energy Eigenaxis Maneuver (ME-EAM) is attained by solving the ME formulation in which the spacecraft's rotational motion is constrained to an EAM.

B. Necessary Conditions For Optimality

Necessary conditions for optimality of the four problem formulations presented in this section may be derived through an application of Pontryagin's Minimum Principal (PMP). Once the necessary conditions are determined, the candidate optimal control solutions, returned by DIDO, may be numerically analyzed for optimality through the application of the co-vector mapping theorem [27–29]. Only the necessary conditions for the off-eigenaxis minimum energy problem, given in Eq. (18), are considered in this section. The ME formulation for eigenaxis maneuvering (ME-EAM), as well the STM formulations, are each derived analogously to the derivations for Eq. (18).

At the heart of the PMP is the Hamiltonian Minimization Condition (HMC), which provides a necessary condition concerning the optimality of the control $u = \tau_{rw}$. The HMC requires, that for an extremal control

u^* to be optimal, u^* must minimize the control Hamiltonian at each instance of time. Because the control Hamiltonian is time invariant, the HMC for problem ME (off-eigenaxis maneuvering) is given as

$$\text{(HMC)} \begin{cases} \text{Min:} & H(\lambda,x,u) = \mathcal{P}^{rgn}_{elec}(x,u) + [\lambda_q{}^\intercal, \lambda_\omega{}^\intercal, \lambda_\Omega{}^\intercal] \begin{bmatrix} \frac{1}{2}\mathcal{Q}(\omega)q \\ J_{sc}^{-1}(-Au - \omega \times (J_{sc}\omega + AJ_{rw}\Omega_{rw})) \\ J_{rw}^{-1}u \end{bmatrix} \\ \text{Subject to:} & \\ & -\omega_{max} \le \omega_i \le \omega_{max} \quad \forall\, i = 1,2,3 \\ & -\Omega_{max} \le \Omega_i \le \Omega_{max} \quad \forall\, i = 1,\ldots,N_{rw} \\ & -\tau_{max} \le u_i \le \tau_{max} \quad \forall\, i = 1,\ldots,N_{rw} \end{cases}$$

where $\lambda_q \in \mathbb{R}^4, \lambda_\omega \in \mathbb{R}^3, \lambda_\Omega \in \mathbb{R}^{N_{rw}}$ are the costate variables for the respective states.

To develop necessary conditions for the HMC, the Karush-Kuhn-Tucker (KKT) conditions are applied through building the Lagrangian of the Hamiltonian, $\overline{H}$. For problem ME,

$$\overline{H}_{ME}(\mu_\omega, \mu_\Omega, \mu_u, \lambda, x, u) = H(\lambda, x, u) + \mu_\omega \omega + \mu_\Omega \Omega + \mu_u u,$$

where $\mu \triangleq \begin{bmatrix} \mu_\omega & \mu_\Omega & \mu_u \end{bmatrix}^\intercal \in \mathbb{R}^{3+2N_{rw}}$ contains the KKT multipliers associated with the HMC (see [2]). Concerning the ME formulation, first order necessary conditions for optimality require that each component of ω, Ω, u and the associated KKT vectors satisfy the complementarity conditions:

$$\mu_{\omega_i} \begin{cases} \le 0 & \omega_i = -\omega_{max} \\ = 0 & -\omega_{max} < \omega_i < \omega_{max} \\ \ge 0 & \omega_i = \omega_{max} \end{cases} \quad \mu_{\Omega_i} \begin{cases} \le 0 & \Omega_{rw,i} = -\Omega_{max} \\ = 0 & -\Omega_{max} < \Omega_{rw,i} < \Omega_{max} \\ \ge 0 & \Omega_{rw,i} = \Omega_{max} \end{cases} \quad \mu_{u_i} \begin{cases} \le 0 & u_i = -\tau_{max} \\ = 0 & -\tau_{max} < u_i < \tau_{max} \\ \ge 0 & u_i = \tau_{max} \end{cases}$$

Along with the necessary conditions given by the complementarity conditions, another set of necessary conditions is arrived upon by considering the lower Hamiltonian. The lower Hamiltonian, $\mathcal{H}$, is acquired by evaluating the control Hamiltonian along an extremal solution, u^*, of the HMC. That is

$$\mathcal{H}(\lambda, x) \triangleq H(\lambda, x, u^*).$$

Since the control Hamiltonian for each of the four problem formulations is time invariant, the Hamiltonian Evolution Condition states that candidate optimal solutions are such that the lower Hamiltonian is constant for all time; that is

$$\frac{d}{dt}\mathcal{H}(\lambda, x) = 0 \qquad \text{for all } t \in [0, T].$$

Along with verifying the necessary conditions for a candidate optimal control solution u^*, demonstrating the feasibility of u^*, and hence the validity of u^*, is a crucial step when analyzing numerical solutions. Feasibility analysis is carried out by propagating the interpolated control from u^* through the dynamics given in Eq. (18) using a standard Runge-Kutta (RK) integrator. An extremal control u^* is deemed feasible if and only if the solution returned by the RK integrator coincides with the solution returned by DIDO. To demonstrate that the necessary conditions for optimality of the ME formulation are satisfied, problem ME was solved in DIDO for a candidate rest-to-rest slew: A 180 degree rotation about the spacecraft's z-body axis, whose attitude parameters are given as $q^0 = [0, 0, 1, 0]^\intercal$ and $q^f = [0, 0, 0, 1]^\intercal$, along with spacecraft parameters given in the Appendix. The transfer time to complete the maneuver was bounded by $T = 307$ seconds. Figure 1 displays the necessary conditions being satisfied for this candidate maneuver for both the lower Hamiltonian and complementarity condition on ω_2: The lower Hamiltonian $\mathcal{H}$ is constant throughout the duration of the maneuver, and ω_2 saturates when $\mu_{\omega_2} \neq 0$. Only the complementarity for ω_2 has been depicted, since profiles for the other spacecraft body axes are similar, and so are omitted for brevity. The additional necessary conditions given by the PMP, such as the Terminal Transversality and Hamiltonian Value Conditions, while each verified, have been omitted for reasons of brevity.

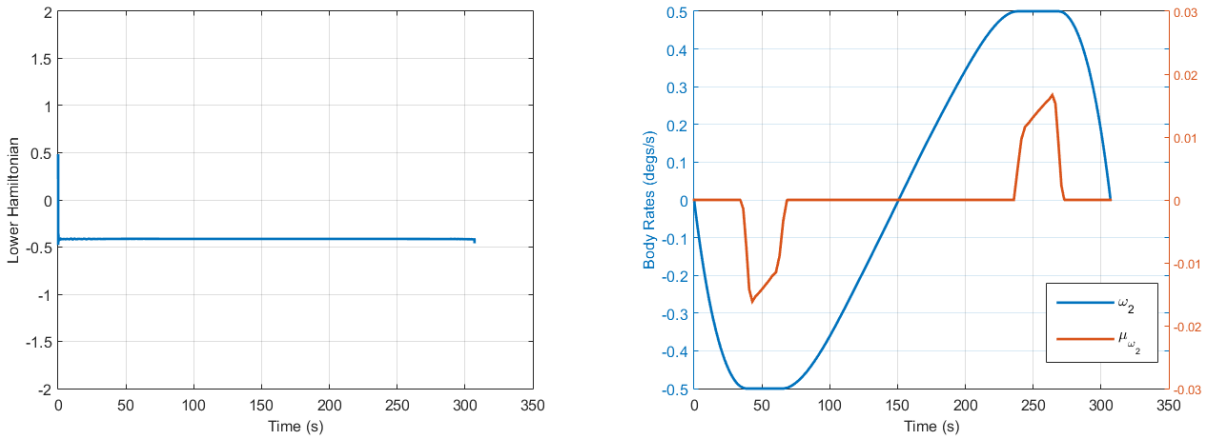

(a) Consistancy of the Lower Hamiltonian $\mathcal{H}$

(b) Complementarity condition for ω_2

Figure 1. Necessary Conditions for problem ME with transfer time bounded-above by 307 seconds.

C. Comparisons to the Shortest-Time Maneuver

In this section, a maneuver attained from solving the standard shortest-time problem formulation is compared to a maneuver attained by solving the ME formulation where the transfer time is bounded at t_{STM}. The results of the comparison depict that time-optimal maneuvers are not unique with respect to energy consumed to perform the slew for both off-eigenaxis and eigenaxis maneuver types.

Shortest-time maneuvers, recently spanning out from theory and into application by being implemented in flight,[10–12] are time-optimal attitude maneuvers based on optimal control theory. Characterized by building up the body-rates of all three spacecraft body axes simultaneously, STMs maximize the agility of a spacecraft by taking full-advantage of the inertia ellipsoid, nonlinear rotational dynamics, and the operational constraints imposed upon the nonlinear rotational dynamics. Table (1) presents the transfer time and energy metrics to both the STM, and the ME-STM. The state and control profiles for each of these agile maneuvers are presented in Figures 2 and 3.

The main result in the comparison between a standard STM and a ME-STM maneuver depicted in Table (1) is, that STMs are not unique with respect to energy, as seen by the difference in the $\mathcal{E}^{+}_{elec}$ metric between the two maneuvers. Both the STM and ME-STM perform the slew in 279.9 seconds, but the ME-STM is able to reduce energy costs by approximately 11% when compared to the standard STM. The cost functional to the ME problem formulation is the summation of the copper and friction loss terms given in Eqs. (16) and (17). Therefore the ME-STM produces a time-optimal slew in which less energy is lost as heat. By an application of Eq. (9), and recalling that optimization is invariant under scalar multiplication, the cost functional to the ME formulation may be written as

$$\int_0^{t_f} \sum_{i=1}^{N_{rw}} \left(\tau_{rw,i}^2(t) + \left(\beta^2 + \frac{\beta K_T^2}{R} \right) \Omega_{rw,i}^2(t) \right) dt.$$

Consulting Table (1), the savings of the ME formulation are due to the substantial reductions in friction loss. By expending a marginal amount of torque, as seen by the 2% increase in copper loss, the reaction wheels are placed in a profile which substantially lower friction costs while producing indistinguishable spacecraft body velocity profiles and attitude profiles (see Figures 2 and 3).

Maneuver Type	$\mathcal{E}^{+}_{elec}$ (J)	$\mathcal{E}^{rgn}_{elec}$ (J)	$\mathcal{C}_{loss}$ (J)	$\mathcal{F}_{loss}$ (J)
STM	162.0	136.3	79.7	56.6
ME-STM	143.9 (-11.2%)	121.0 (-11.2%)	81.3 (+1.9%)	39.7 (-29.8%)

Table 1. Metrics to the Shortest-Time Maneuver and Minimal Energy Shortest-Time Maneuver for the 180 degree slew about the spacecraft z-body axis. Values in parenthesis represent percentage change.

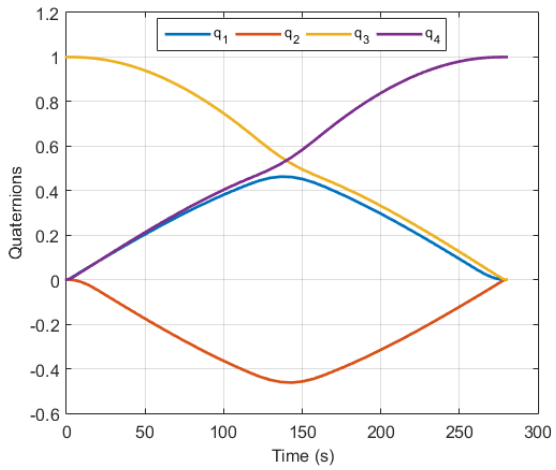

(a) Shortest-Time Maneuver q

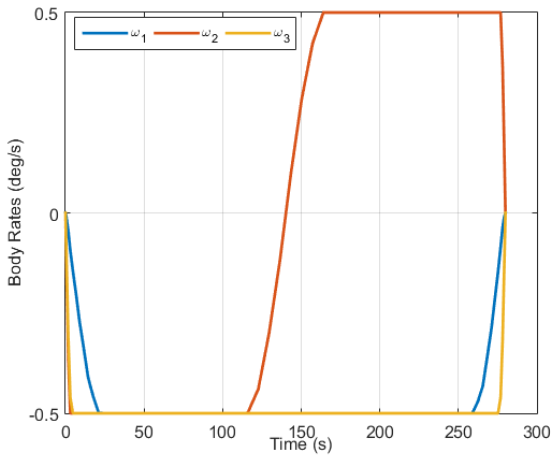

(b) Shortest-Time Maneuver ω

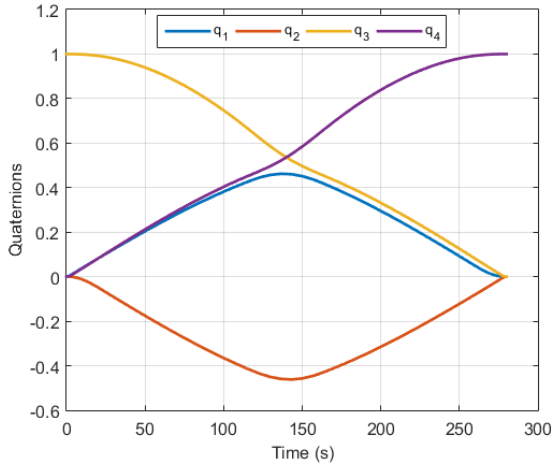

(c) Minimum Energy Shortest-Time Maneuver q

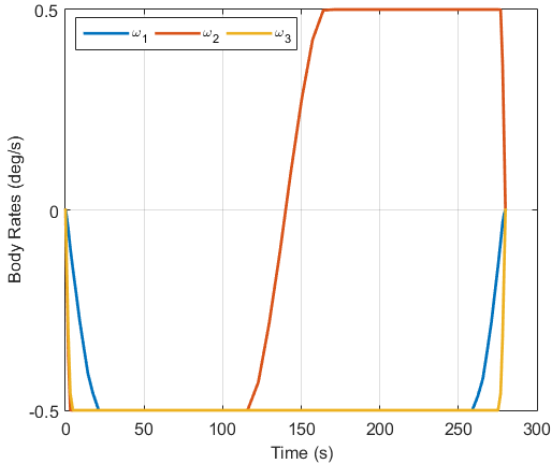

(d) Minimum Energy Shortest-Time Maneuver ω

Figure 2. Shortest-Time Maneuver and Minimum Energy Shortest-Time Maneuver quaternion, q, and spacecraft angular velocity, ω, profiles for the large angle slew simulation are the same.

The fact that there exists a difference in energy between shortest-time and minimal energy shortest-time, signifies that shortest-time maneuvers are not unique with respect to energy consumption. The state-control pairs attained by solving the canonical STM formulation may be improved upon, with respect to energy, through solving the ME formulation, which may be considered as refining the shortest-time solutions, via a minimum energy control allocation. Such re-allocation of the control is possible because there exists a nontrivial null space to the matrix A which projects the reaction wheel motor-torques onto the spacecraft body. Because of the nontrivial null space, there exists an infinite number of distinct motor-torques which produce null-motions. The standard shortest-time formulations simply search for feasible trajectories which seek to minimize the transfer time, without regard to energy consumption. By solving the ME-STM, maneuvers are determined which complete in the same transfer time yet incur a smaller cost with respect to energy consumption. Therefore, in a situation in which time-optimal maneuvering is required, the control-scheme attained from the ME formulation should be applied in lieu of a standard STM. We also note that control re-allocation can also be used to improve the efficiency of conventional eigenaxis maneuvers.

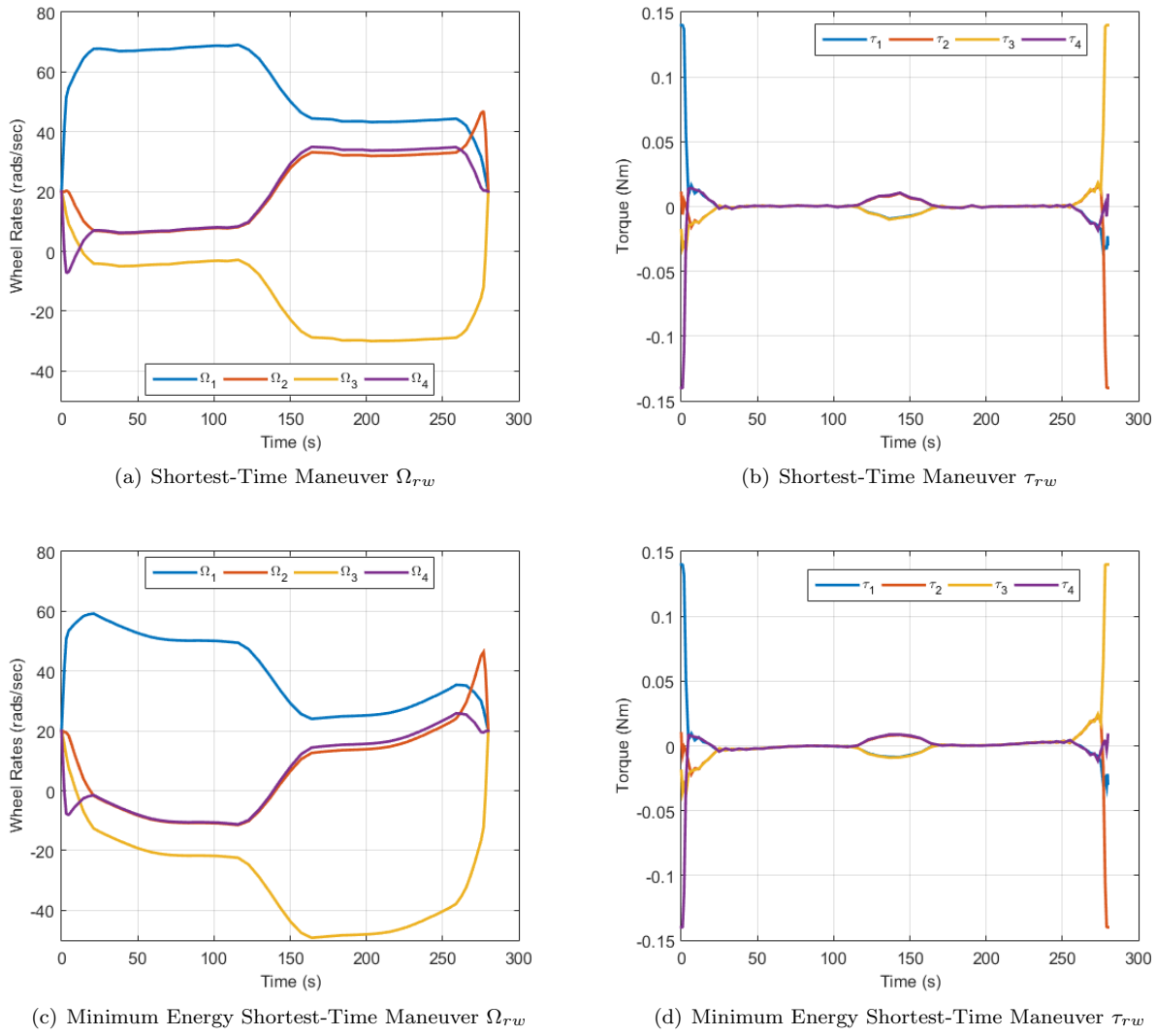

(a) Shortest-Time Maneuver Ω_{rw}

(b) Shortest-Time Maneuver τ_{rw}

(c) Minimum Energy Shortest-Time Maneuver Ω_{rw}

(d) Minimum Energy Shortest-Time Maneuver τ_{rw}

Figure 3. Shortest-Time Maneuver and Minimum Energy Shortest-Time Maneuver reaction wheel angular velocity, Ω_{rw}, and control, τ_{rw}, profiles for the large angle slew simulation.

IV. The Relationship Between Transfer Time and Minimal Energy

The purpose of this section is to identify the relationship between transfer time and the minimal energy required to perform a slew for both eigenaxis and off-eigenaxis maneuvering. By identifying the energy/time relationships, the shortest-time maneuver satisfying a given energy budget may be identified, and a comparison may be made between on and off-eigenaxis maneuvering concerning energy and transfer time. In determining the relationship, a 180 degree slew about the spacecraft's z-body axis is first considered, whose initial and final quaternions are $q^0 = [0, 0, 1, 0]^\intercal$ and $q^f = [0, 0, 0, 1]^\intercal$. Following the single-slew analysis, the minimal-energy and transfer-time relationship is analyzed in a typical setting for an imaging satellite: a multipoint maneuver consisting of a sequence of five slews.

A. Off-Eigenaxis Slew Analysis

With the determination of the shortest-time maneuver from Section III, the lower time-bound in which the rest-to-rest slew may be performed is attained. Next, by solving a series of ME formulation of fixed times T, a Pareto Front is generated which depicts the minimal energy required to perform the slew for a given transfer time. This Pareto front for off-eigenaxis maneuvering is given in Figure 4. Since the

ME formulation minimizes $\mathcal{E}_{elec}^{rgn}$, the red curve in Figure 4 represents the minimal energy cost for a given slew time. Recall the cost function used assumes 100% regeneration of waste energy. The actual energy consumption $\mathcal{E}_{elec}^{+}$ is calculated a posteriori is shown as the blue curve. We note that the optimal cost always slightly underestimates the energy used and forms a lower bounding curve.

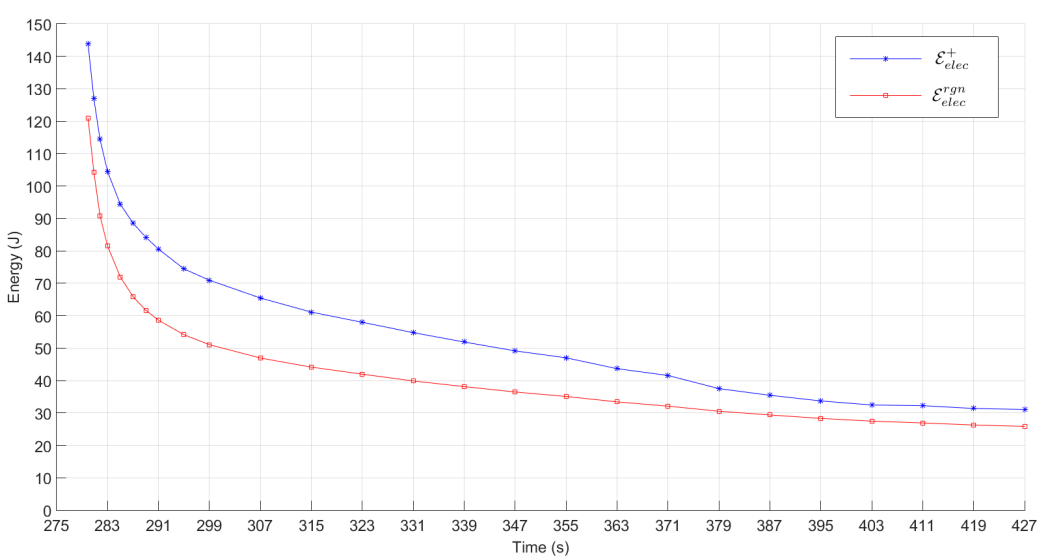

Figure 4. Pareto Fronts of the 180 degree z-body-axis for energy-minimal off-eigenaxis maneuvering for the energy-metrics $\mathcal{E}_{elec}^{+}$ (blue) and $\mathcal{E}_{elec}^{rgn}$ (red).

With the aid of the visualization provided by the Pareto front, the nonlinear relationship between the transfer time and the minimal energy required to perform the slew is observed to consist of three phases when viewing time increasing from the shortest-time. Firstly, as transfer time is decreased to the shortest-time, there exists a time window in which the energy required to perform the maneuver begins to asymptotically increase. Denoting this portion of the Pareto front as the head, this window of asymptotic growth about the shortest-time may be identified with the time interval $[t_{STM}, 295]$. Secondly: The relationship in Figure 4 showcases that there exists a point in time where savings in energy by increasing transfer time significantly diminish. Defining this portion of the Pareto front as the tail, this time window may be defined as the interval $[395, \infty)$. Lastly, a third portion of the Pareto front may be identified simply as the region in between the head and tail of the Pareto Front $[295, 395]$, and depicts that energy decays roughly proportionally to increasing transfer times.

The behavior of energy with respect to time within the head portion of the Pareto front validates the intuition that shortest-time maneuvers can be costly maneuvers with respect to energy. More notably though, the head of the Pareto front signifies that small increases in transfer time from the shortest-time net significant savings in energy. In other words, there exists near time-optimal maneuvers which cost much less than the ME-STM counterpart. Thus it is possible to balance energy and transfer time requirements when missions demand an agile setting.

The tail-portion of the Pareto front in Figure 4 is inversely analogous to the head region. Whereas small increases in transfer time near t_{STM} net substantial savings in energy in the head region, increases in transfer time within the tail portion of the Pareto front net only minor savings in energy. While the Pareto front of Figure 4 stops with a transfer time of 427 seconds, the energy and time relationship in the tail section continues in like-manner for all time, slowly decaying over large intervals of time. Therefore, in a setting where transfer time is of no concern, the tail-portion of the energy-time relationship depicts that there is not much benefit from significantly increasing the transfer time of a maneuver with respect to energy consumption.

B. Eigenaxis Slew Analysis

With the ME-EAM formulation along with the shortest-time EAM, a Pareto front describing the minimal energy transfer time relationship with respect to eigenaxis maneuvering may be built analogously to the Pareto front constructed in Section IV.A. The result of this construction is given in Figure 5, and has been superimposed upon Pareto front of Figure 4. For each of the curves in Figure 5 the minimal-energy is reported as the $\mathcal{E}^{+}_{elec}$ metric.

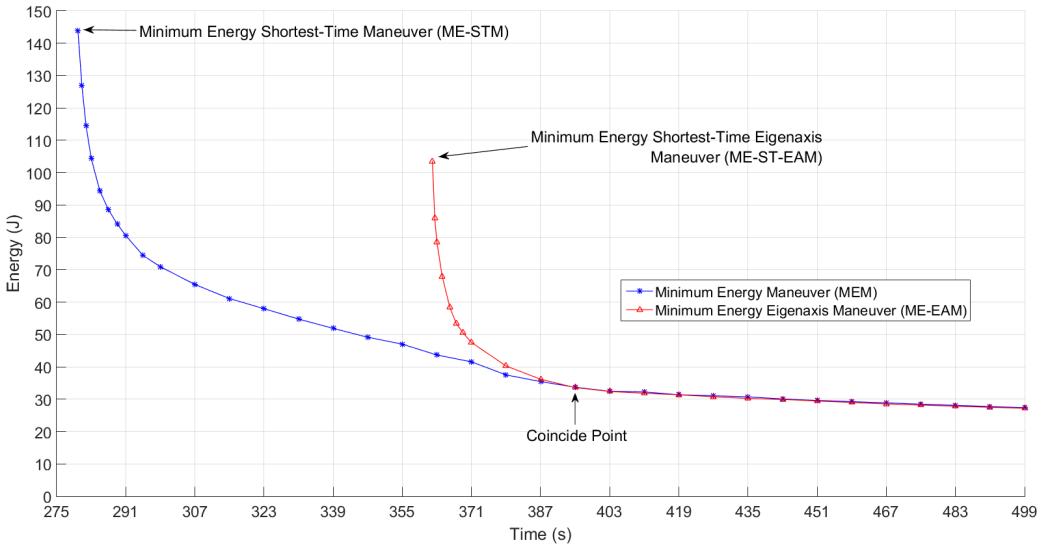

Figure 5. Pareto Fronts of the 180 degree z-body-axis for energy-minimal off-eigenaxis and eigenaxis maneuvering. Transfer time (in seconds) is along the horizontal axis, and the vertical access is the energy (given by $\mathcal{E}^{+}_{elec}$) required to perform the slew in the alloted transfer time.

From Figure 5, a direct comparison between the two maneuver types may be made with respect to transfer time and energy. Figure 5 clearly depicts that the minimal energy EAM curve lies completely encompassed within the region defined by the off-eigenaxis curve for all time. Both maneuver types coincide with respect to energy for all slews which have a transfer time $T \geq 395$ seconds. This coincide point depicts that there exists a point in transfer time in which on-and off-eigenaxis maneuver types are equivalent with respect to energy consumption. In other words, the minimum energy slew is an eigenaxis maneuver.

The EAM Pareto front depicts an analogous relationship with respect to energy and transfer time compared to the off-eigenaxis Pareto front. Namely, near the shortest-time (for an eigenaxis maneuver), energy costs significantly increase, depicting that there exist maneuvers with a near time optimal transfer time that incur much significantly less energy costs.

From the time optimal transfer time t_{STM}, of 279.9 seconds, to the coincide point of 395 seconds, the two Pareto fronts in Figure 5 depict the existence of a trade space between transfer time as well as energy between eigenaxis and off-eigenaxis maneuvering. A geometric argument may be made in discerning a trade off between the two maneuver types: An energy budget may be visualized with a horizontal line in Figure 5, and in like manner, a vertical line visualizes a time budget. Figure 6 explores the trade-space with respect to transfer time between EAMs and off-eigenaxis maneuvers in a setting in which the energy consumed by the spacecraft when executing eigenaxis maneuvering is acceptable to mission requirements. The horizontal lines in Figure 6 depict that, for every minimal energy eigenaxis slew, there exists an off-eigenaxis maneuver with a smaller transfer time for a given energy. The extreme case with respect to transfer time is is identified in Figure 6 by the maneuver which is energy equivalent to the ME-ST-EAM. Table (2) depicts the energy metrics and time for the energy equivalent maneuver to the ME-ST-EAM along with the metrics to the ME-ST-EAM for reference. In this case, by maneuvering off-eigenaxis, it is possible to decrease the transfer time by 21.7% (from 362.0 seconds to 283.1 seconds) while consuming the same amount of energy as an minimal energy eigenaxis maneuver (103.5 J), a counter intuitive result. Comparing to shortest-time maneuvering, for same amount of energy required to perform a ME-ST-EAM, the transfer time may be brought within 1%

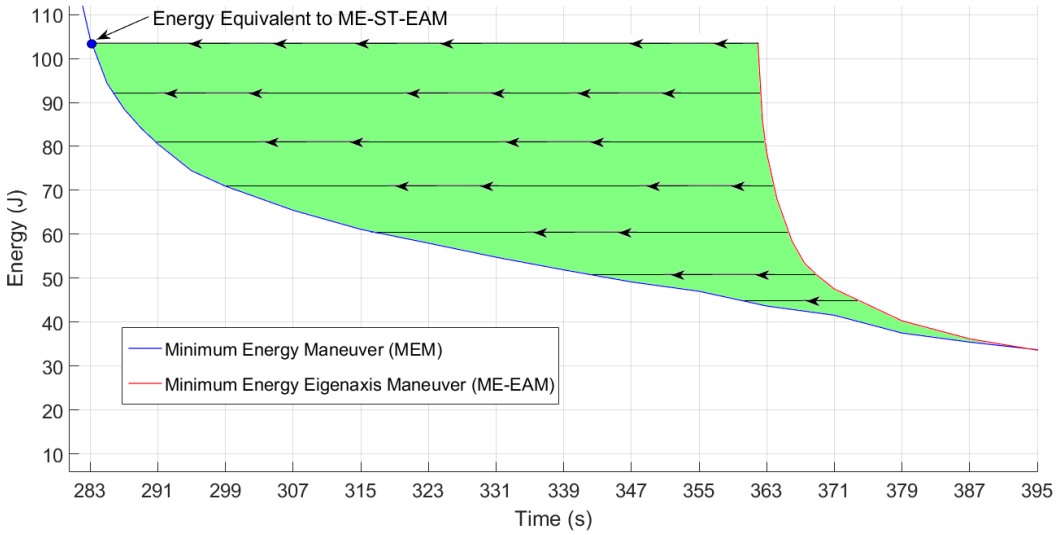

Figure 6. Trade space depicting the benefit of off-eigenaxis maneuvers with respect to energy: For each eigenaxis maneuver, there exists an off-eigenaxis maneuver with a lower transfer time for the same energy budget as the eigenaxis maneuver.

of t_{STM} by maneuvering off-eigenaxis. Therefore, the transfer time may be substantially reduced by control re-allocation.

Maneuver Type	TT (s)	$\mathcal{E}^{+}_{elec}$ (J)	$\mathcal{E}^{rgn}_{elec}$ (J)	$\mathcal{C}_{loss}$ (J)	$\mathcal{F}_{loss}$ (J)
ME-ST-EAM	362.0	103.5	91.4	68.5	22.9
Energy Equivalent to ME-ST-EAM	283.1 (-21.7%)	103.5 (0.0%)	80.8 (-11.6%)	42.7 (-37.7%)	38.2 (+66.8%)

Table 2. Metrics to the Minimal Energy Shortest-Time Eigenaxis Maneuver, and energy equivalent off-eigenaxis maneuver, for the 180 degree slew about the spacecraft z-body axis. Values in parenthesis represent percentage change.

Figure 7 depicts that, in the case where EAM transfer times are acceptable to meet mission requirements, the energy can be substantially reduced by control re-allocation. The extreme case identified in Figure 7 is the off-eigenaxis maneuver which completes in the same transfer time as the time-optimal minimum energy eigenaxis maneuver (ME-ST-EAM). By being able to maneuver off-eigenaxis, the most agile EAM transfer time (of 362.0 seconds) requires 57.5% less energy (from 103.5 J to 44.0 J) that would be required to achieve the eigenaxis maneuver. Therefore, by maneuvering the spacecraft off-eigenaxis energy may be substantially reduced when compared to conventional eigenaxis maneuvering, another counter intuitive result.

Maneuver Type	$\mathcal{E}^{+}_{elec}$ (J)	$\mathcal{E}^{rgn}_{elec}$ (J)	$\mathcal{C}_{loss}$ (J)	$\mathcal{F}_{loss}$ (J)
Transfer Time Equivalent to ME-ST-EAM	44.0 (-57.5%)	33.6 (-63.2%)	8.6 (-87.4%)	25.1 (+9.6%)

Table 3. Metrics to the off-eigenaxis maneuver which is transfer time equivalent to the Minimal Energy Shortest-Time Eigenaxis Maneuver, for the 180 degree slew about the spacecraft z-body axis. Values in parenthesis represent percentage change to the Minimal Energy Shortest-Time Eigenaxis Maneuver.

Figure 8 depicts the boresight traces (aligned to the spacecraft y-axis) for on and off eigenaxis maneuvers for the 180 degree z-body-axis slew. As expected, the eigenaxis maneuver traces out the shortest angular path, as represented by the straight-line path between the two orientations. Similarly as expected, the boresight traces of the ME-STM, and the maneuver which is equivalent in energy to the minimal-energy shortest-time eigenaxis maneuver each depict off-eigenaxis maneuvers by deviating from the circular arc traced by the EAM.

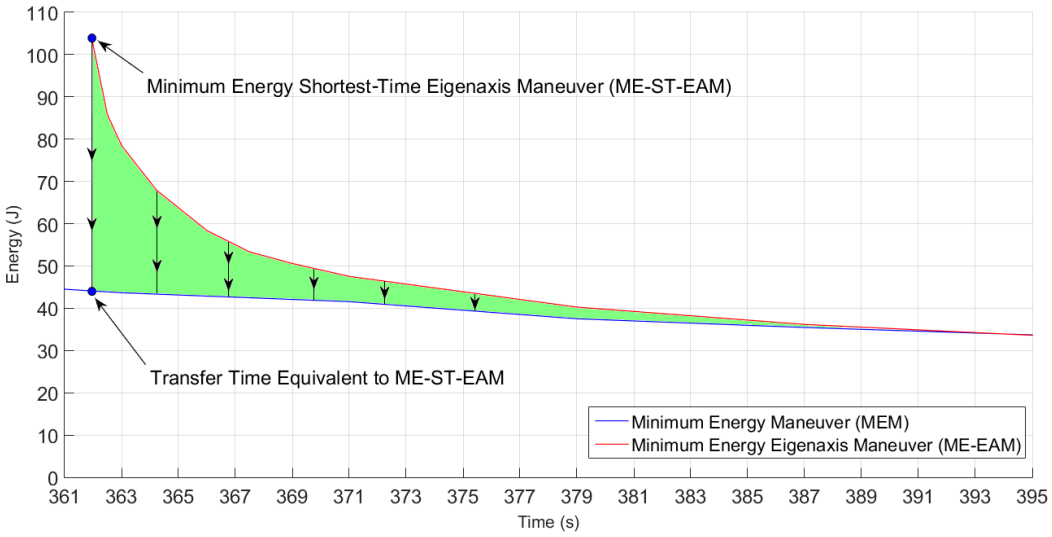

Figure 7. Trade Space depicting the benefit of off-eigenaxis maneuvers with respect to transfer time: For each eigenaxis maneuver, there exists an off-eigenaxis maneuver with a lower energy budget completing in the same transfer time as the eigenaxis maneuver.

C. Operational Scenario

This section expands upon the analysis of the previous sections, by considering a multipoint slew consisting of five maneuvers. A multislew maneuver is considered here to demonstrate that the properties resultant from the analysis of the single slew directly translate to a typical operational scenario for an imaging spacecraft involving multiple collection points. The five-point multislew is based off of the STAR pattern developed in [11], and consists of reorienting the imaging boresight (aligned with the spacecraft y-axis) over both medium angle ($\approx$30) and large angle ($\gg$ 30) slews. The relevant attitude parameters for both on-and off-eigenaxis maneuvering for the five-point multislew are given in Table (4).

Orientation	q_1	q_2	q_3	q_4
1	0.0602	0.1850	0.6165	0.7629
2	0.2860	0.0069	0.5607	0.7770
3	0.1864	0.0045	0.0854	0.9788
4	0.1195	0.1431	0.7921	0.5812
5	0.1314	0.1263	0.2458	0.9520
6	0.1693	0.0781	0.4666	0.8646

Table 4. Sequence of quaternions for the five-point multislew maneuver.

Four maneuver types are selected to explore the trade space between energy and transfer time between on and off eigenaxis maneuvering: i,ii) The ME-STM and ME-ST-EAM which represent the minimal energy required to complete the multislew for time optimal off and on eigenaxis maneuver types iii) The (off-eigenaxis) maneuvers which are energy equivalent (with respect to $\mathcal{E}^{+}_{elec}$) to each minimal energy time optimal eigenaxis maneuver (ME-ST-EAM) iv) The off-eigenaxis maneuvers which are equivalent with respect to transfer times of the ME-ST-EAMs. Figure 9 depicts each of the four maneuver types in a conceptualized Pareto front to demonstrate how these four corner points will serve to explore the trade space of energy and time for EAMs and off-eigenaxis maneuvers. Table (5) contains the totals for transfer time and energy metrics to perform the five-point multislew for four different maneuver types, and Table (6) depicts the percentage change of the transfer time and energy metrics when opting between the various agile and conventional maneuver strategies. As expected from intuition, the ME-STMs, compared to their time optimal EAM counterparts ME-ST-EAMs, are able to decrease transfer time by 19.6% (from 649.4 seconds to 522.0 seconds)

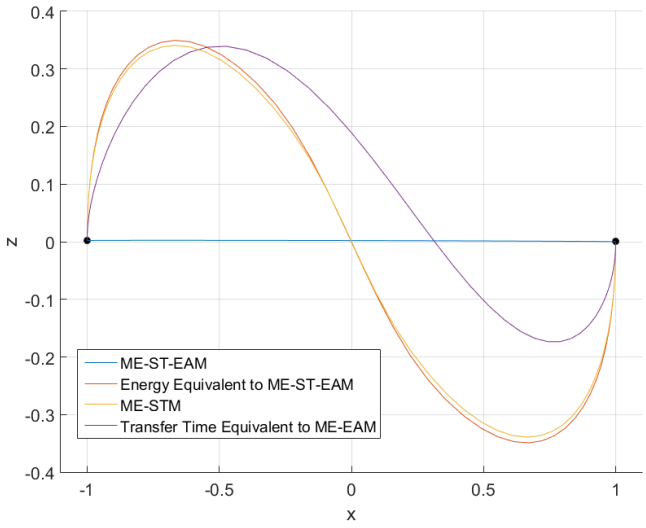

Figure 8. Boresight traces for various maneuver-types performing a 180 degree z-body-axis slew.

but at the cost of increasing energy consumption by 124% (from 409.6 J to 918.5 J). Because each individual slew has an energy and transfer time relationship between eigenaxis and off-eigenaxis maneuvering akin to the single slew analyzed in Section IV, there exist agile maneuvers (e.g. smaller transfer time than eigenaxis maneuvering) with significantly less demanding energy requirements. By maneuvering off-eigenaxis, for the same energy budget as the ME-ST-EAMs, the multislew may be completed within 5.7% of the time optimal transfer time (from 522.0 seconds to 551.9 seconds) while consuming 55.6% less energy than the ME-STMs (from 918.5 J to 408.6 J). Similarly, by allowing off-eigenaxis maneuvering, for the same energy budget as the ME-ST-EAMs, the transfer time of the ME-ST-EAMs may be reduced by 15% (from 649.4 seconds to 551.9 seconds). Considering the situation of minimizing energy, the transfer-time equivalent maneuver-set is able to decrease the energy requirements of the ME-ST-EAMs by 53% while completing the multislew with the same transfer time taken by the ME-ST-EAMs, having the lowest energy requirements of the four representative maneuvers in Table (6) of only 191.4 J. Viewing the four representative maneuver-types together, the energy-equivalent and transfer-time equivalent off-eigenaxis maneuvers depict that there exists a significant penalty in time and energy when enforcing eigenaxis rotations. By allowing the spacecraft to maneuver off-eigenaxis, the optimization may take full advantage of the attitude control-capability as represented by the spacecraft agilitoid.[3]

Maneuver Type	TT (s)	$\mathcal{E}^{+}_{elec}$ (J)
ME-STM	522.0	918.5
Energy Equivalent to ME-ST-EAM	551.9	408.6
ME-ST-EAM	649.4	409.6
Transfer Time Equivalent to EAMs	649.4	191.4

Table 5. Transfer times and metric totals for the four maneuver-types to the five-point multislew.

Change of Maneuver Type	%Δ TT	$\%\Delta\mathcal{E}^{+}_{elec}$
ME-ST-EAM $\longrightarrow$ ME-STM	-19.6%	+124.2%
ME-STM $\longrightarrow$ Energy Equivalent to ME-ST-EAM	+5.7%	-55.5%
ME-ST-EAM $\longrightarrow$ Energy Equivalent to ME-ST-EAM	-15.0%	-0.2%
ME-ST-EAM $\longrightarrow$ Transfer Time Equivalent to EAMs	0%	-53.3%

Table 6. Percentage change opting between various maneuver types in Table (5) for the multipoint slew.

The boresight trace over the course of the five-point multislew are given in Figure 10 for the ME-STM, ME-ST-EAM, along with the energy-equivalent and transfer-time equivalent off eigenaxis maneuvers in Figure 11. The imaging boresight for the ME-ST-EAM, as expected, traces out shortest-circular arcs between the five capture-locations. Similarly expected, from Figure 10a, the motion of the boresight to the ME-STMs deviates from the eigenaxis for each of the five orientations. For reference, the boresight trace to the STMs are identical to those given in Figure 10a. Similarly, the energy equivalent and transfer time equivalent maneuvers depict that the entire multipoint slew is performed off-eigenaxis. That the traced-path between each of the five orientations for the three off-eigenaxis maneuver-types are each distinct, is due to the combination of the boundary conditions as well as the inertia properties of the spacecraft. Since the rotational-maneuvers are not restricted about an eigenaxis, the optimization may minimize energy by taking full advantage of the spacecraft's geometry per the boundary conditions when determining a feasible slew.

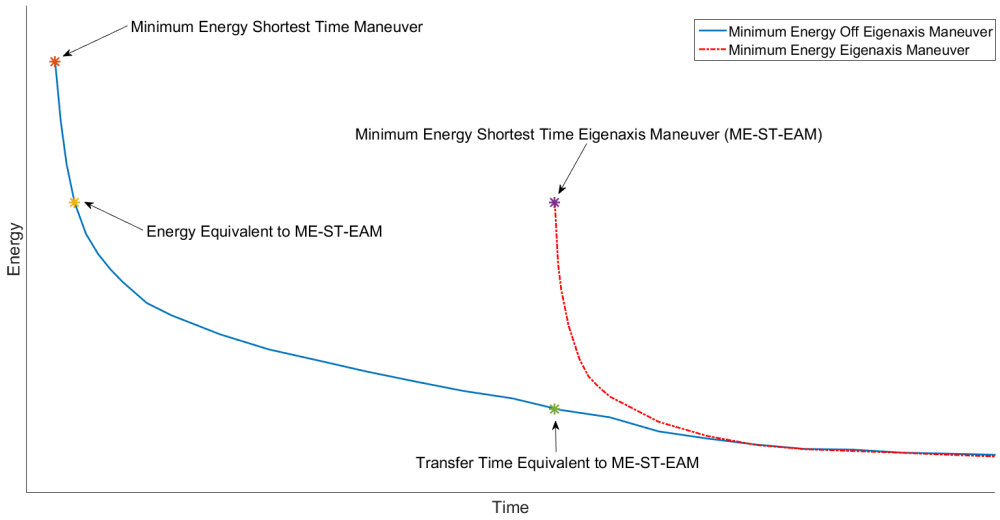

Figure 9. Conceptual visualization of the four maneuver types selected to explore the energy and transfer time trade space between on-and off-eigenaxis maneuvering for the operational scenario of a five-point multislew.

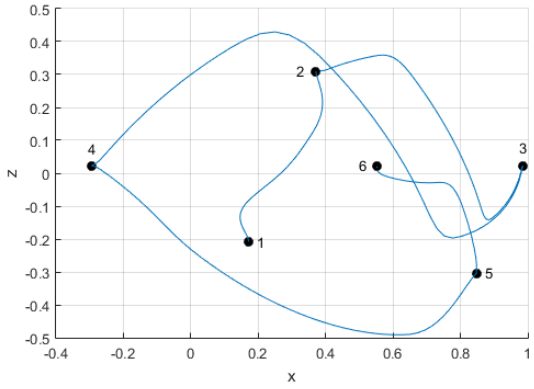

(a) Minimum Energy Shortest-Time Maneuver

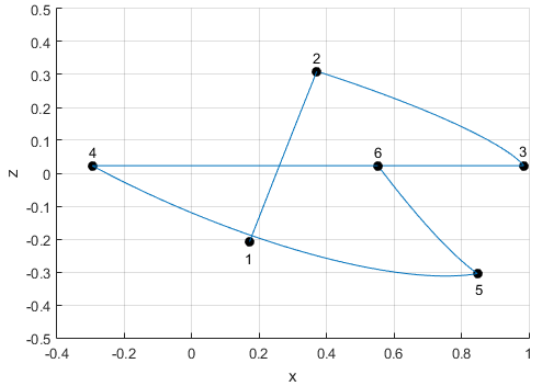

(b) Minimum Energy Shortest-Time Eigenaxis Maneuver

Figure 10. Boresight Traces to two of the four maneuver-types from Table (5).

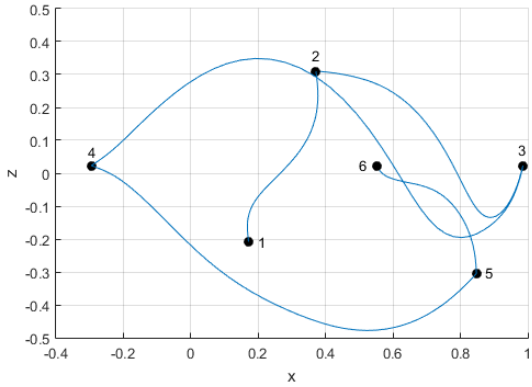

(a) Energy Equivalent to Minimum Energy Shortest-Time Eigenaxis Maneuver

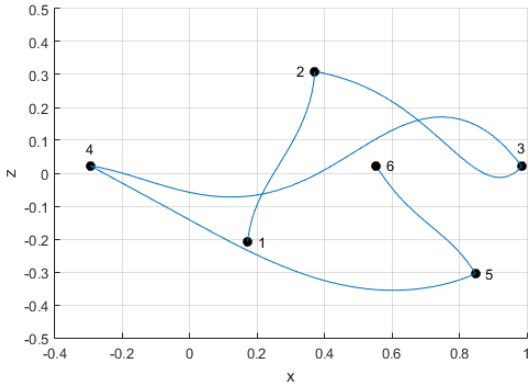

(b) Transfer Time Equivalent to Minimum Energy Shortest-Time Eigenaxis Maneuver

Figure 11. Boresight Traces to two of the four maneuver-types from Table (5).

V. Conclusion

In this paper, a new approach to minimum energy attitude control was taken by modeling the reaction wheels as DC motors in steady state. This gave energy metrics that are in-line with the true operational cost of performing a slew. These metrics were then embedded into a new optimal control problem formulation to minimize the energy required to perform a rest-to-rest slew for both eigenaxis and off-eigenaxis maneuvering-types. The optimal control problem was subsequently solved using Legendre pseudospectral methods implemented in the software package DIDO. Simulation results for a single large-angle slew and then for a five-point multislew implemented as eigenaxis and off-eigenaxis maneuver-types, depicted that for spacecrafts utilizing a redundant number of RWs, both time-optimal EAMs and off-eigenaxis maneuvers are not unique with respect to energy. The open-loop state-control pair solutions attained by solving the ME problem formulations mitigate the demanding energy costs associated with the solutions attained solving standard STM formulations, by substantially reducing the energy lost due to friction. Therefore providing a desirable alternative for settings which demand time optimal maneuvering. Simulations also showed a host of results allowing a greater understanding of the cost-relationships between energy and agility when executing slews:

1. There exists a nonlinear relationship between transfer time and minimal energy consumed, with STMs consuming the most energy. This relationship, invariant under both eigenaxis and off-eigenaxis maneuvering, depicts two key results: i) There exists near time optimal maneuvers which require significantly less energy than STMs, therefore providing desirable alternatives to STMs in a setting where agility is needed under energy constraints and ii) There exists a point in transfer time in which little benefit to reducing energy by increasing transfer time, therefore depicting that there is little merit to increasing the transfer time past a certain point in an effort to reduce energy requirements. This is due to the shallow tail of the Pareto front.

2. Performing an eigenaxis maneuver, although widely used, severely constrains the attitude control system with respect to transfer time as well as energy. There exists a trade space in which, by maneuvering off-eigenaxis, transfer time may be significantly decreased for the same energy-cost as an eigenaxis maneuver. Similarly, another trade space exists in which, by maneuvering off-eigenaxis, the energy may be greatly decreased for the same transfer time as an eigenaxis maneuver. The savings are realized by re-allocating the control effort. As transfer time is increases for a slew, eventually there exists a point in transfer time in which off-EA and EA maneuvering coincide with respect to energy for the rest of time. This point of coincide depicts that for large-enough transfer time, off-eigenaxis maneuvering is equivalent to eigenaxis maneuvering. Similarly, the coincide point identifies the point at which large increases in transfer time net small savings with respect to energy.

The simulations presented here illustrate that the proposed optimal control strategy is able to improve upon the manner in which STMs are performed, as well as reduce the energy requirements for conventional slews.

Appendix

The spacecraft parameters used in this paper are presented below in Table (7).

Parameter	Symbol	Value
Number of reaction wheels	N_{rw}	4
Armature resistance	R	1.8 Ohms
Torque constant	K_T	0.0696 Nm/A
Back EMF constant	K_V	$0.0696\ \mathrm{V}\cdot(\mathrm{rads/s})^{-1}$
Viscous friction coefficient	β	$4.3\times10^{-5}\ \mathrm{Nm}\cdot(\mathrm{rads/s})^{-1}$
Reaction wheel wheel-speed bias	Ω_{bias}	$\begin{bmatrix}20 & 20 & 20 & 20\end{bmatrix}^{\intercal}$ rads/s
Maximum angular velocity of spacecraft body axis	ω_{max}	0.5 degs/s
Maximum angular velocity of a reaction wheel	Ω_{max}	449.9808 rads/s
Maximum motor torque	τ_{max}	0.14 Nm/s
Inertia of the N_{rw} reaction wheels	J_{rw}	$\mathrm{diag}\Big(\begin{bmatrix}0.012 & 0.012 & 0.012 & 0.012\end{bmatrix}\Big)\ \mathrm{kg}\cdot\mathrm{m}^2$
Reaction wheel projection matrix	A	$\begin{bmatrix}\frac{1}{\sqrt{3}} & -\frac{1}{\sqrt{3}} & -\frac{1}{\sqrt{3}} & \frac{1}{\sqrt{3}}\\ \frac{1}{\sqrt{3}} & -\frac{1}{\sqrt{3}} & \frac{1}{\sqrt{3}} & -\frac{1}{\sqrt{3}}\\ \frac{1}{\sqrt{3}} & \frac{1}{\sqrt{3}} & -\frac{1}{\sqrt{3}} & -\frac{1}{\sqrt{3}}\end{bmatrix}$
Spacecraft inertia tensor	J_{sc}	$\begin{bmatrix}59.22 & -1.14 & -0.80\\ -1.14 & 40.56 & 0.10\\ -0.80 & 0.10 & 57.60\end{bmatrix}\ \mathrm{kg}\cdot\mathrm{m}^2$

Table 7. Spacecraft parameters[10,30] used in the problem formulations defined in Section III.

References

[1]I. M. Ross and F. Fahroo, "Legendre Pseudospectral Approximations of Optimal Control Problems," *Kang, W. et al. (eds.) Lecture Notes in Control and Information Sciences*, Vol. 295, pp. 327–342, Springer, New York, 2003.

[2]I. M. Ross, *A Primer on Pontryagin's Principle in Optimal Control, second edition.* Collegiate Publishers, San Francisco, CA, 2015.

[3]I. M. Ross and M. Karpenko, "A Review of Pseudospectral Optimal Control: from Theory to Flight," *Annual Reviews in Control*, Vol. 36, No. 2, 2012, pp. 182–197.

[4]Q. Gong, W. Kang, and I. M. Ross, "A Pseudospectral Method for the Optimal Control of Constrained Feedback Linearizable Systems," *IEEE Transactions on Automatic Control*, Vol. 51, No. 7, 2006, pp. 1115–1129.

[5]W. Kang, Q. Gong, I. Ross, and F. Fahroo, "On the convergence of nonlinear optimal control using pseudospectral methods for feedback linearizable systems," *International Journal of Robust and Nonlinear Control*, Vol. 17, No. 14, 2007, pp. 1251–1277.

[6]I. M. Ross, R. J. Proulx, M. Karpenko, and Q. Gong, "Riemann-Stieltjes Optimal Control Problems for Uncertain Dynamical Systems," *Journal of Guidance, Control, and Dynamics*, Vol. 38, July 2015, pp. 1251–1263.

[7]N. Bedrossian, S. Bhatt, M. Lammers, L. Nguyen, and Y. Zhang, "First Ever Flight Demonstration of Zero Propellant Maneuver Attitude Control Concept," *Guidance, Navigation, and Control Conference*, Hilton Head, South Carolina, 2007, pp. AIAA–2007–6734.

[8]N. S. Bedrossian, S. Bhatt, W. Kang, and I. M. Ross, "Zero-propellant Maneuver Guidance," *IEEE Control Systems Magzine*, Vol. 29, No. 5, 2009, pp. 53–73.

[9]W. Kang and N. Bedrossian, "Pseudospectral Optimal Control Theory Makes Debut Flight — Saves NASA $1M in Under 3 hrs," *SIAM news*, Vol. 40, No. 7, 2007.

[10]M. Karpenko, S. Bhatt, N. Bedrossian, A. Fleming, and I. M. Ross, "First Flight Results on Time-Optimal Spacecraft Slews," *Journal of Guidance, Control, and Dynamics*, Vol. 35, No. 2, 2012, pp. 367–376.

[11]M. Karpenko, S. Bhatt, N. Bedrossian, and I. M. Ross, "Flight Implementation of Shortest-Time Maneuvers for Imaging Satellites," *Journal of Guidance, Control, and Dynamics*, 2014, pp. 1–11.

[12]N. Bedrossian, M. Karpenko, and S. Bhatt, "Overclock My Satellite," *IEEE Spectrum*, Vol. 49, No. 11, 2012, pp. 54–62.

[13]H. Schaub and V. J. Lappas, "Redundant Reaction Wheel Torque Distribution Yielding Instantaneous L2 Power-Optimal Spacecraft Attitude Control," *Journal of Guidance, Control, and Dynamics*, Vol. 32, No. 4, 2009, pp. 1269–1276.

[14]R. Blenden and H. Schaub, "Regenerative Power-Optimal Reaction Wheel Attitude Control," *Journal of Guidance, Control, and Dynamics*, Vol. 35, No. 4, 2012, pp. 1208–1217.

[15]W. R. Wehrend, "Minimum Energy Reaction Wheel Control for a Satellite Scanning a Small Celestial Area," NASA TN D-392, 1967.

[16]S. Skaar and L. Kraige, "Single-Axis Spacecraft Attitude Maneuvers Using an Optimal Reaction Wheel Power Criterion," *Journal of Guidance, Control, and Dynamics*, Vol. 5, No. 5, 1982, pp. 543–544.

[17]S. Skaar and L. Kraige, "Large-Angle Spacecraft Attitude Maneuvers Using an Optimal Reaction Wheel Power Criterion," *Journal of the Astronautical Sciences*, Vol. 32, No. 1, 1984, pp. 47–61.

[18]J. L. Junkins and J. D. Turner, "Optimal Continuous Torque Attitude Maneuvers," *Journal of Guidance, Control, and Dynamics*, Vol. 3, No. 3, 1980, pp. 210–217.

[19]H. Schaub, *Analytical Mechanics of Space Systems*. AIAA Education Series, AIAA, Reston, VA, Third ed., 2003.

[20]B. Wie, *Space Vehicle Dynamics and Control*. AIAA Education Series, AIAA, Reston, VA., Second ed., 2008.

[21]F. L. Markley, "Attitude Estimation or Quaternion Estimation?," *Journal of Astronautical Sciences*, Vol. 52, No. 1, 2004, pp. 221–238.

[22]B. Wie and P. M. Barba, "Quaternion Feedback for Spacecraft Large Angle Maneuvers," *Journal of Guidance, Control, and Dynamics*, Vol. 8, No. 3, 1985, pp. 360–365.

[23]M. Yoong, Y. Gan, G. Gan, C. Leong, Z. Phuan, B. Cheah, and K. Chew, "Studies of Regenerative Braking in Electric Vehicle," *Sustainable Utilization and Development in Engineering and Technology (STUDENT), 2010 IEEE Conference on*, IEEE, 2010, pp. 40–45.

[24]X. Nian, F. Peng, and H. Zhang, "Regenerative Braking System of Electric Vehicle Driven by Brushless DC Motor," *IEEE Transactions on Industrial Electronics*, Vol. 61, No. 10, 2014, pp. 5798–5808.

[25]A. Fleming, P. Sekhavat, and I. M. Ross, "Minimum-Time Reorientation of a Rigid Body," *Journal of Guidance, Control, and Dynamics*, Vol. 33, No. 1, 2010, pp. 160–170.

[26]B. Wie and J. Lu, "Feedback Control Logic for Spacecraft Eigenaxis Rotations Under Slew Rate and Control Constraints," *Journal of Guidance, Control, and Dynamics*, Vol. 18, No. 6, 1995, pp. 1372–1379.

[27]Q. Gong, I. M. Ross, W. Kang, and F. Fahroo, "Connections between the covector mapping theorem and convergence of pseudospectral methods for optimal control," *Computational Optimization and Applications*, Vol. 41, No. 3, 2008, pp. 307–335.

[28]I. Ross and Q. Gong, "Emerging Principles in Fast Trajectory Optimization," *Elissar Global, Carmel, CA*, 2010.

[29]I. M. Ross, "A Historical Introduction to the Convector Mapping Principle," *Proceedings of Astrodynamics Specialists Conference*, Monterey, CA, 2005.

[30]E. Ahronovich and M. Balling, "Reaction Wheel and Drive Electronics For LeoStar Class Space Vehicles," 1998.